Exciton Regeneration Dynamics in Model Donor−Acceptor Polymer Heterojunctions

John Glenn S. Ramon and Eric R. Bittner*

Department of Chemistry and Center for Materials Chemistry, University of Houston, Houston, Texas 77204
Received: March 21, 2006; In Final Form: August 17, 2006

We present a theoretical investigation on various semiconducting materials that exhibit photovoltaic and photoluminecent properties. Our focus is on the relaxation dynamics that occur upon photoexcitation of a couple of type II donor−acceptor heterojunction systems. In addition to the diabatic approach our two-band exciton model employs to study the phonon-assisted relaxations, we adopt the Marcus−Hush semiclassical method to incorporate lattice reorganization. This enables us to look at the state-to-state interconversions from the relaxed excited-state configurations in model polymer blends of poly(9,9-dioctylfluorene-*co*-*N*-(4-butylphenyl)diphenylamine) (TFB) with poly(9,9-dioctylfluorene-*co*-benzothiadiazole) (F8BT) and poly(9,9-dioctylfluorene-*co*-bis-*N*,*N*-(4-butylphenyl)-bis-*N*,*N*-phenyl-1,4-phenylenediamine) (PFB) with F8BT. Our results stress the significance of vibrational relaxation in the state-to-state relaxation. Furthermore, while a tightly bound charge-transfer state (exciplex) remains the lowest excited state, we show that the regeneration of the optically active lowest excitonic state in TFB:F8BT is possible via the existence of a steady state.

I. Introduction

Over the past number of years there has been a tremendous burst of progress in developing organic polymer based semiconductor materials for both photovoltaic and light-emitting diode applications. While commercial applications of these material have appeared, future progress in this field hinges upon fundamental research in the fabrication, synthesis, and electronic properties of these materials. Perhaps the most fascinating aspect of research in this area is that it lies very much at the junction of molecular chemistry and condensed and solid-state physics.

In this paper, we consider the relaxation and reorganization dynamics that occur upon photo- or electrostimulation of a series of model organic semiconducting heterojunctions. On the molecular level, these heterojunctions are formed by intermolecular interactions between neighboring chains of conjugated polymers with different electron affinities (EA) or ionization potentials (IP). This generates an intermolecular driving force that can lead to charge-separation if the mismatch between either the IP or EA is greater than the binding energy of an intrachain electron/hole pair (≈0.5−0.6 eV). In our previous paper on this issue,[1] we used a two-band Wannier-function/configuration interaction approach to develop a series of models for three type II semiconducting polymer heterojunction materials that are being explored for photovoltaic and light-emitting diode (LED) applications.[2−4] Our model assumes that the band centers for the π conduction and valence bands can be obtained by considering the relative difference between the EA and IP for the various components and then referencing the offsets to the band centers for poly(*p*-phenylenevinylene) (PPV) determined by band-structure calculations. The band offsets for each of the junctions are shown in Figure 1.

In the case of the PPV:BBL junction, both bands are offset by more than ∼0.5 eV. Consequently, photoexcitation of *either* the PPV or BBL will result in efficient charge separation. In this case, the charge-separated state will be with the hole localized on the PPV and the electron on the BBL chain. This efficient separation of charges across the heterojunction suggests

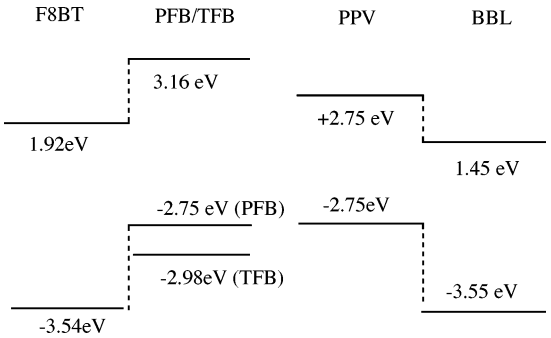

Figure 1. Relative band offsets for the various type II junctions considered in these series of papers. BBL = poly(benzimidazobenzophenanthroline ladder), PPV = poly(*p*-phenylenevinylene), F8BT = poly(9,9-dioctylfluorene-*co*-benzothiadiazole), PFB = poly(9,9-dioctylfluorene-*co*-bis-*N*,*N*-(4-butylphenyl)-bis-*N*,*N*-phenyl-1,4-phenylenediamine), and TFB = poly(9,9-dioctylfluorene-*co*-*N*-(4-butylphenyl)-diphenylamine).

that the PPV:BBL polymer blend is an ideal candidate for light-harvesting devices such as solar cells.[5,6]

PFB:F8BT and TFB:F8BT junctions have been shown to exhibit photovoltaic as well as photoluminescent behavior to varying degrees.[7,8] Both straddle the exciton destabilization threshold. In PFB:F8BT, the offset in the valence band is greater than the exciton binding energy and the lowest energy excited state will have the electron localized on the F8BT and the hole on the PFB. TFB, on the other hand, is chemically very similar to PFB but with a higher ionization potential resulting in a lower lying valence band. Consequently, the valence band offset is almost equal to the exciton binding energy and the lowest lying excitation has some intrachain exciton character.[1]

In this paper, we continue along the lines established therein and consider the state-to-state relaxation dynamics that occur upon either charge-injection into an LED material or photoexcitation of a photovoltaic material. Two photophysical pathways are developed. First is one in which the state-to-state relaxation occurs in the framework of a fixed nuclear geometry (the diabatic approach). Second, we present a new approach for computing the state-to-state relaxation dynamics between the

* Address correspondence to this author. E-mail: bittner@uh.edu.

10.1021/jp061751b CCC: $33.50
Published on Web 09/20/2006

adiabatically relaxed excited states (the Marcus−Hush approach). Our results stress the significance of lattice reorganization and show that while the more tightly bound charge-transfer state (exciplex) remains the lowest excited state in these heterojunction systems, the optically active lowest excitonic state may be regenerated.

In the next section, we present a summary of the two-band exciton model. We also elaborate on the diabatic and the Marcus−Hush methods adopted to calculate the interconversion rates and the implication of each approach on the electron/hole dynamics of the systems we look at. In Section III, we compare and contrast the two approaches. Here, we look at the relaxation dynamics of the essential excited states by looking at their time-evolved populations. We examine the role of lattice reorganization and the effect of temperature on these interconversions and show how these affect the fluorescence of the material.

II. State-to-State Relaxation

A. Summary of the Model. We adopt the model for the on-chain electronic excitations of a single conjugated polymer chain[2−4] to describe our heterojunction systems. Essentially, this model uses localized valence and conduction band Wannier functions[WFs] ($|\bar{h}\rangle$ and $|p\rangle$) to describe the π-orbitals and two weakly interacting phonon branches to describe the bond stretches and torsions of the polymer backbone. In addition, coupling between the electronic excitations and the lattice phonons is accounted for empirically. The overall Hamiltonian is

$$\mathrm{H} = \sum_{mn}(F^{\mathrm{o}}_{mn} + V_{mn})A_m^{\dagger}A_n + \sum_{\mathrm{nmi}\mu}\left(\frac{\partial F^{\mathrm{o}}_{nm}}{\partial q_{i\mu}}\right)A_n^{\dagger}A_m q_{i\mu} + \sum_{i\mu}(\omega_\mu^{\,2}(q_{i\mu}^{\,2} + \lambda_\mu q_{i\mu}q_{i+1,\mu}) + p_{i\mu}^{\,2}) \quad (1)$$

consisting of electronic terms (first sum), H_{el}, phonon terms (third sum), H_{ph}, and electron−phonon coupling terms (second sum), $H_{\mathrm{el-ph}}$. $A_n^{\dagger}$ and A_n are creation and annihilation operators acting upon the ground electronic state, $|0\rangle$, giving rise to electron/hole configurations, $|n\rangle = |\bar{h}p\rangle$, with the hole localized at h and the electron at p. Further, $q_{i\mu}$ and $p_{i\mu}$ are the lattice distortions and momentum components in the ith site and μth phonon branch.

In the domain of single chain systems,[2] the single-particle matrix elements, F^{o}_{mn}, are given by

$$F^{\mathrm{o}}_{mn} = \delta_{m_h n_h} f_{m_e n_e} + \delta_{m_e n_e}\bar{f}_{m_h n_h} \quad (2)$$

where $f_{mn}(\bar{f}_{mn})$ are the localized energy levels (site energies for $m = n$) and nearest-neighbor transfer integrals ($t_{||}$ for $m = n \pm 1$) of the electrons (holes). The two-particle matrix elements, V_{mn}, are given by the two-body integrals J_r (Coulomb attraction),[9] K_r (spin-exchange),[10] and D_r (transition dipole−dipole coupling).[11] These two-body integrals are determined by the linear intersite distance, $r = r_{||}$, according to

$$J_r = J_0(1 + r/r_0)^{-1} \quad (3)$$

$$K_{\mathrm{r}} = K_0 \exp(-r/r_0) \quad (4)$$

$$D_r = D_0(r/r_0)^{-3} \quad (5)$$

where $J_0 = 3.0921$ eV with $r_0 = 0.6840$, $K_0 = 1.0574$ eV with $r_0 = 0.4743$, and $D_0 = -0.0321$ eV with $r_0 = 1.0$. The r_0 values correspond to a unit screening length given in terms of an arbitrary lattice displacement, a.

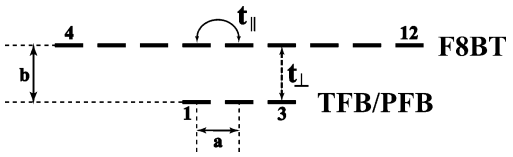

Figure 2. Site model scheme for a two parallel chain heterojunction.

While our focus here is to model heterojunction systems, we emphasize that the various parameters used were individually tuned and verified to agree with independent studies of single chain systems. For instance, the electron and hole site energies for each of the chemical species were determined by comparing their ionization potentials (IP) and electron affinities (EA) to that of PPV. By further introducing modulation of the valence and conduction band site energies for each chain, the electron and hole become localized within each copolymer unit. This is consistent with what has been observed in previous studies by Karabunarliev et al.,[3] Cornil et al.,[12] and Jespersen et al.[13] on copolymer chains with alternating donor−acceptor units. In particular, when applied to an isolated F8BT chain, we have shown,[1] among others, that the absorption spectrum gives two distinct peaks that are consistent with the calculations of Jespersen et al.[13] and observations of Stevens et al.[14] This leads us to believe we have a reasonable estimate of the band offsets at the interface between the two semiconducting polymers of each heterojunction.

Since we are interested in π-stacked parallel chain systems, we consider the following approximations (refer to Figure 2). First, in addition to the intrachain hopping integrals, $t_{||}$, we introduce interchain hopping integrals, $t_\perp$, to describe the interchain site couplings. As with $t_{||}$, we consider only nearest-neighbor transfer integrals. Further, we approximate $t_\perp$ to be 0.01 eV as compared to ∼0.5 eV for $t_{||}$. This value is in agreement with the calculations by Vogl and Campbell[15] and Yu et al.[16] Second, we take the interchain two-body interactions J_r, K_r, and D_r to have the same functional form as in the intrachain case with $r = r_\perp$ being the linear distance between two interchain sites. Since there is greater dielectric screening between two chains compared to two repeat units on the same chain, these interchain interactions are expected to be weaker than the intrachain interactions. Thus, we take the interchain separation, b, to be somewhat greater than the lattice displacement, a. Systematic variations of the interchain separation are found to affect the CI eigenenergies of the lowest excited states to a sizable extent. We have tuned this interchain separation to correspond to the observed exciton-exciplex energy splitting for PFB:F8BT and TFB:F8BT. These approximations are discussed in detail in our previous paper.[1]

For the case of parallel chains, we assume that there is no direct mechanical coupling between the chains. Consequently, each polymer chain is assumed to possess its own ensemble of phonon normal modes localized on the given chain and that there are no interchain phonon−phonon couplings. Moreover, since we have assumed bilinear coupling between on-site displacement coordinates $q_{i\mu}$ and hard-wall boundary conditions, the phonon normal-mode frequencies for each mode ξ are given by

$$\omega_{\xi\mu}^{\,2} = \omega_\mu^{\,2} + 2\lambda_\mu \cos\left(\frac{\xi\pi}{2(N+1)}\right) \quad (6)$$

where N is the number of lattice sites in a given chain, ω_μ the band center for the μ-phonon band, λ the coupling, and $\xi = 1$,

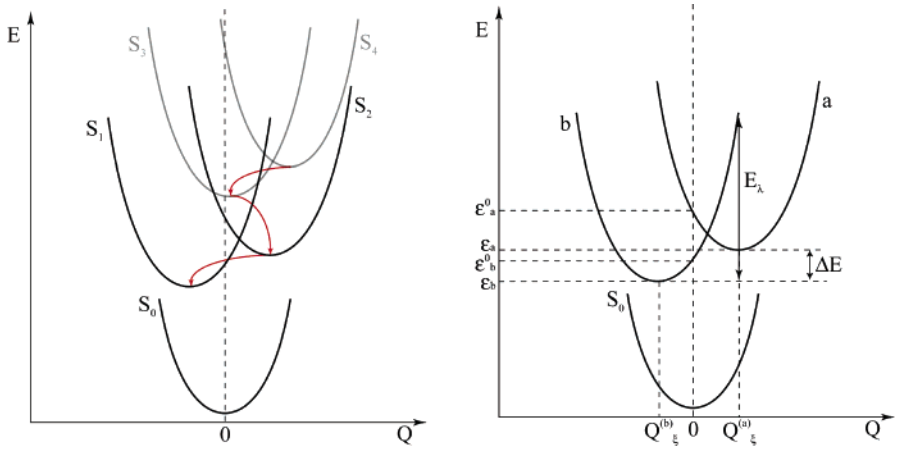

Figure 3. Illustration of diabatic potential energy curves along one normal mode coordinate: (a) the relaxed state-to-state interconversions and (b) the vertical and relaxed state energies as well as the Marcus parameters.

..., N. In what follows, we shall condense our notation and adopt a generic ξ to denote both normal mode and band.

Finally, an important component in our model is the coupling between the electronic and lattice degrees of freedom. These we introduce via a linear coupling term of the form

$$\left(\frac{\partial f_{mn}}{\partial q_{i\mu}}\right)^0 = \frac{S_\mu}{2}(2\hbar\omega_\mu{}^3)^{1/2}(\delta_{mi} + \delta_{ni}) \tag{7}$$

where S_μ is the Huang−Rhys factor that can be obtained from the vibronic features in the experimental photoemission spectrum. The Huang−Rhys factor, S, is related to the intensity of the $0-n$ vibronic transition

$$I_{0-n} = \frac{e^{-S}S^n}{n!} \tag{8}$$

For the case of conjugated polymers such as PPV and similar poly(phenylene-vinylene) species, the emission spectra largely consist of a series of well-resolved vibronic features corresponding to the C═C stretching modes in the phenylene rings with typical Huang−Rhys factors of $S = 0.6$ and a broad featureless background attributed to either low-frequency ring torsions (in the case of phenylene-vinylene polymers) or other low-frequency modes with weak coupling to the electronic states with $S_\mu \approx 4$. On the other hand, the photoluminescence spectra of F8 shows a series of well-resolved vibronic peaks with an energy separation of about 1600 cm^{-1}.[14,17,18] Analysis of the Huang−Rhys factors of F8 in crystalline β-phase and glassy states indicates a relatively low overall Huang−Rhys factor of $S = 0.6$,[17] which indicates that there is relatively little geometric relaxation following the transition from the excited to the ground state in these systems. This value of $S = 0.6$ is also in reasonable agreement with values estimated by Guha et al. for ladder-type poly-*p*-phenylene and $S = 1.2$ for *p*-hexaphenyl.[19] The modes which would couple a more planar excited state to a nonplanar ground state involve torsions between phenylene rings. These low-frequency modes occur at around 70 cm^{-1} and cannot be spectroscopically resolved.[17,20] On the basis of these observations it seems reasonable from the standpoint of model building that two phonon branches, one with $\omega = 1600$ cm^{-1} and $S = 0.6$ and the other with $\omega = 70$ cm^{-1} and $S = 4$, provide a transferable set of electron/phonon couplings suitable for the conjugated polymers considered in this work.

Diagonalization of H_{el} and H_{ph} yields vertical excited states, $|a^0\rangle$, with energies, ϵ_a^0, and normal modes, Q_ξ, with frequencies, ω_ξ, that allow us to express H in the diabatic representation

$$H = \sum_a \epsilon_a^0 |a^0\rangle\langle a^0| + \frac{1}{2}\sum_\xi (\omega_\xi^2 Q_\xi^2 + P_\xi^2) + \sum_{ab\xi} g_{ab\xi}^0 Q_\xi (|a^0\rangle\langle b^0| + |b^0\rangle\langle a^0|) \tag{9}$$

where $g_{ab\xi}^0$ is the diabatic coupling between the orthogonal vertical states $|a^0\rangle$ and $|b^0\rangle$.

Iterative minimization of the potential energies, $\epsilon_a(Q_\xi)$, according to the self-consistent equations

$$\frac{\partial \epsilon_a(Q_\xi)}{\partial Q_\xi} = \frac{\partial\langle a|H|a\rangle}{\partial Q_\xi} = g_{aa\xi}(Q_\xi) + \omega^2{}_\xi Q_\xi = 0 \tag{10}$$

yields relaxed excited states, $|a\rangle$, with energies ϵ_a. This gives a system of displaced harmonic potential energy surfaces (PES) (see Figure 3b) in normal coordinates

$$\epsilon_a(Q_\xi) = \epsilon_a + \frac{1}{2}\sum_\xi \omega_\xi^2 (Q_\xi - Q_\xi^{(a)})^2, \tag{11}$$

where $Q_\xi^{(a)}$ are the normal mode coordinates at the relaxed state $|a\rangle$ configuration given by

$$Q_\xi^{(a)} = -\frac{g_{aa\xi}}{\omega^2{}_\xi} \tag{12}$$

The coupling, $g_{ab\xi}$ (without the superscript 0), between relaxed states $|a(Q_\xi^{(a)})\rangle$ and $|b(Q_\xi^{(b)})\rangle$ are derived from the nonorthogonal transformation of the diabatic couplings, $g_{ij\xi}^0$, obtained from eq 9,

$$g_{ab\xi} = \sum_{ij} S_{ai}^\dagger g_{ij\xi}^0 S_{bi} \tag{13}$$

where a and b refer to the relaxed states while i and j refer to the vertical states such that

$$S_{ai} = \langle i|a(Q_\xi^{(a)})\rangle \tag{14}$$

is the overlap integral between the relaxed state $|a(Q_\xi^{(a)})\rangle$ and

the vertical state $|i\rangle$. Here, we note that the relaxed states $|a(Q_\xi^{(a)})\rangle$ and $|b(Q_\xi^{(b)})\rangle$ are eigenstates of different Hamiltonians (i.e., corresponding to different geometric configurations) and, as such, are generally nonorthogonal.

B. Relaxation Dynamics. *1. Internal Conversions in the Diabatic Approximation.* The nonradiative decay in polymeric systems is predominated by the intramolecular vibrational relaxation (IVR). In our previous papers,[3,21,22] internal conversions were handled in the diabatic approximation,

$$k_{ab}^{\mathrm{IC}} = \pi \sum_\xi \frac{(g_{ab\xi}^0)^2}{\hbar\omega_\xi}[1+\eta(\omega_{ab})] \times [\Gamma(\omega_\xi - \omega_{ab}) - \Gamma(\omega_\xi + \omega_{ab})] \quad (15)$$

where $\omega_{ab} = (\epsilon_a^0 - \epsilon_b^0)/\hbar$ is the transition frequency and η is the Bose−Einstein distribution. Here, for elementary one-phonon transitions to occur, there must be a mode, ω_ξ, close to the transition frequency, ω_{ab}. While this provides a way to integrate the phonon modes in the relaxation, it does so in the limit of having a fixed nuclear configuration, specifically, that of the ground-state nuclear configuration.

2. Internal Conversions in the Marcus−Hush Approach. After photoexcitation of conjugated polymers, rapid thermalization or vibrational energy redistribution sets in. While this remains to be a conjecture based on indirect evidence as noted by Lanzani et al.,[23−25] there is ample reason to believe that this is true in light of the polymeric systems having many more vibrational modes available.[26] This suggests electronic transitions occur from the relaxed excited-state configurations rather than from the $Q_\xi = 0$.

To account for the interconversions from the relaxed excited-state configurations (see Figure 3a), we consider a semiclassical approach based on the Marcus−Hush approximation.[27,28] The internal conversion rate from a thermalized state manifold can be derived from the Golden Rule rate formula of quantum mechanics

$$k_{ab} = \frac{2\pi}{\hbar}\int \mathrm{d}Q\, f(\epsilon_a(Q_\xi))|V_{ab}|^2 \delta(\epsilon_a(Q_\xi) - \epsilon_b(Q_\xi)) \quad (16)$$

where $f(\epsilon_a(Q_\xi))$ is the thermal distribution function of the initial state, V_{ab} is the transition matrix element, and $\epsilon_{a/b}(Q_\xi)$ are the energies at Q_ξ given by eq 11. Generally, V_{ab} is dependent on the nuclear degrees of freedom; however, if we assume its coordinate dependence to be negligible, we apply the Condon-Approximation and take it to be the purely electronic coupling, $g_{ab\xi}$. In the high-temperature limit, this equation transforms into[29]

$$k_{ab}^{\mathrm{IC}} = \left(\frac{\pi}{\hbar^2 k_{\mathrm{B}} T E_\lambda}\right)^{1/2} \exp\left(-\frac{(\Delta E - E_\lambda)^2}{4E_\lambda k_{\mathrm{B}} T}\right) \times \sum_\xi |g_{ab\xi}|^2 \quad (17)$$

where ΔE is the driving force,

$$\Delta E = \epsilon_a - \epsilon_b \quad (18)$$

and E_λ is the reorganization energy given by

$$E_\lambda = \sum_\xi \frac{\omega_\xi^2}{2}(Q_\xi^{(b)} - Q_\xi^{(a)})^2 \quad (19)$$

Here, $Q_\xi^{(a)}$ and $Q_\xi^{(b)}$ refer to the normal mode coordinates of the relaxed lattice configurations of states *a* and *b*, respectively.

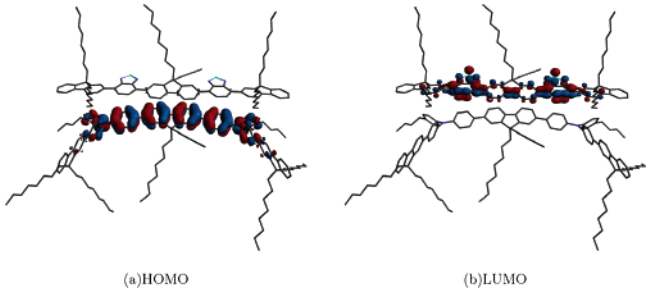

Figure 4. Semiempirical (PM3) LUMO and HOMO wave functions for TFB:F8BT showing the LUMO localized at F8BT(upper chain) while the HOMO localized at TFB (lower chain).

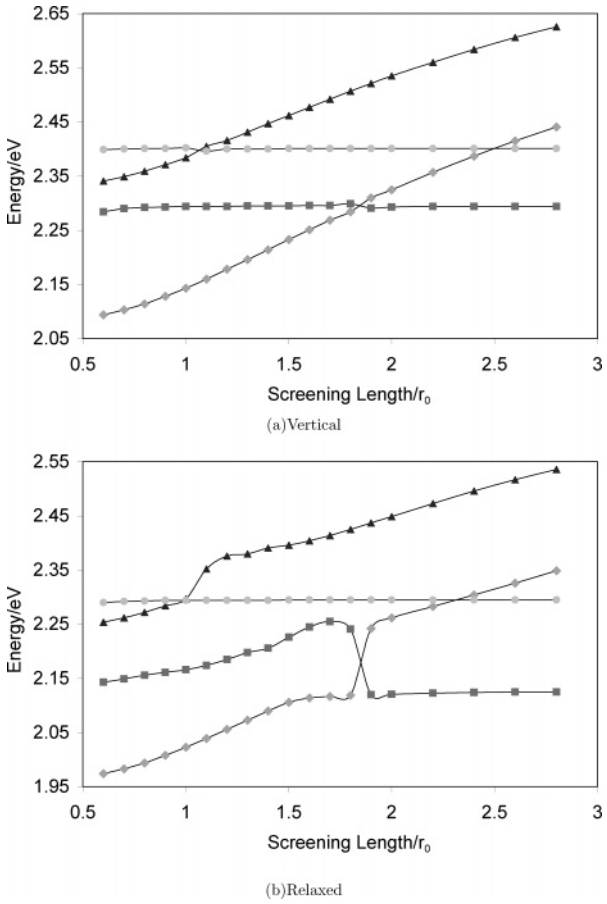

Figure 5. Lowest (a) vertical and (b) relaxed CI eigenstate energies of TFB:F8BT as a function of the interchain screening length given in terms of r_0. In both instances, the CT states (solid diamonds and triangles) are more sensitive to the screening length than the XT states (solid squares and circles).

The $g_{ab\xi}$ are the coupling between relaxed states calculated in eq 13. We further note that the diabatic coupling typically enforces e−h symmetry whereas the adiabatic/Marcus−Hush rates allow transitions between even and odd parity blocks. Barford et al. has elegantly described the parity of singlet and triplet particle-hole excitations through their symmetry.[30] This has implications especially with regards to the spin-dependence of the dissipative dynamics in conjugated polymers and the experimentally observed conjugation length dependence of the ratio of the singlet versus triplet exciton formation rates.[21]

III. Calculations and Discussion

Semiempirical (MM3[31]/PM3[32]) calculations for a 5 copolymer TFB:F8BT (3 dioctylfluorene units on each chain) (Figure 4)

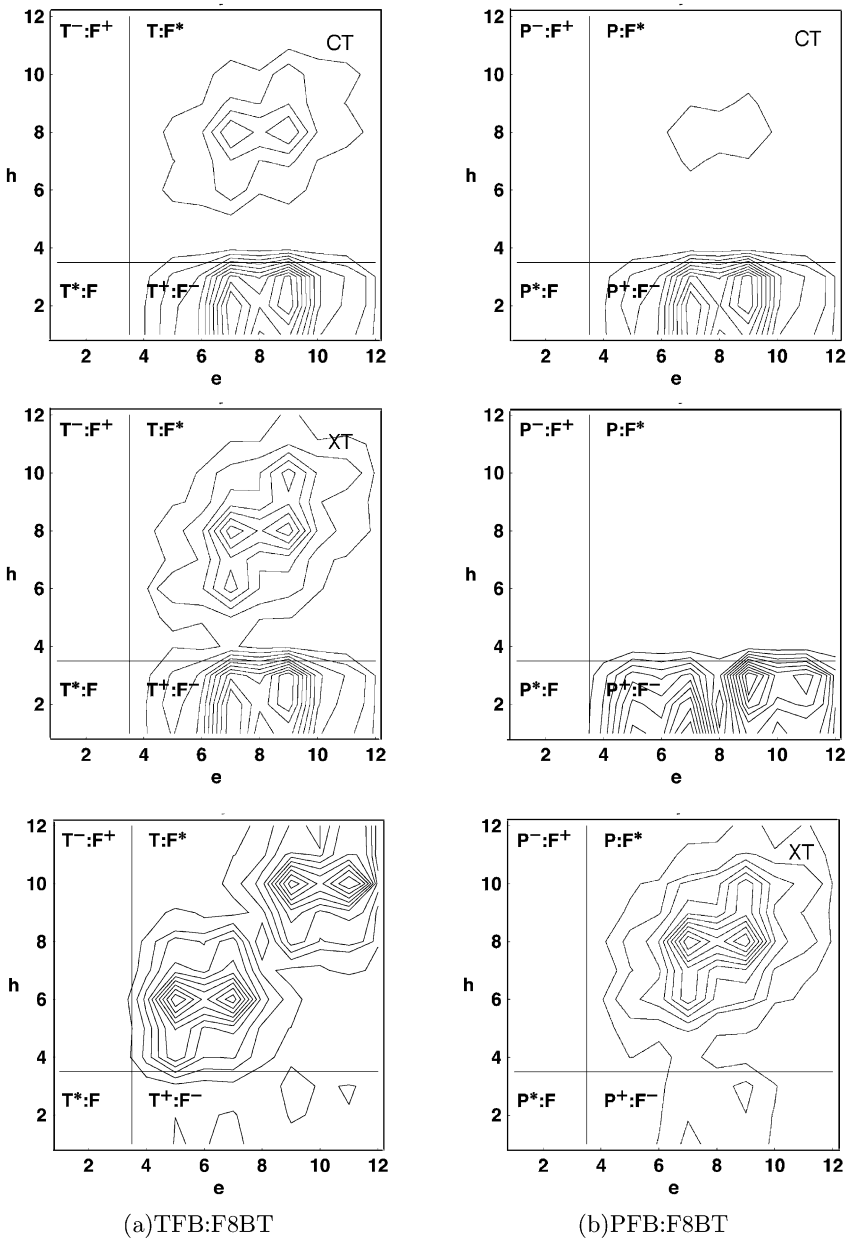

Figure 6. Electron/hole densities of the three lowest adiabatically relaxed excited states for (a) TFB:F8BT and (b) PFB:F8BT. The axes "e" and "h" refer to the electron and hole "coordinates" on the lattice, respectively, with sites 1−3 being TFB or PFB 4−12 being F8BT sites as labeled in Figure 2. Each quadrant is labeled as $T^-:F^+$, T:F*, $T^+:F^-$, and T*:F where T = TFB, P = PFB, F = F8BT, − = electron, + = hole, and * = exciton.

clearly show the HOMO wave function localized at TFB while the LUMO wave function localized at F8BT. While F8BT is rodlike, the presence of triphenylamines in TFB limits the cofacial configuration over approximately three units of the corresponding copolymer chains. Thus we consider a configuration of 3 copolymer units for TFB and 9 copolymer units of F8BT as shown in Figure 2 in our subsequent simulations.

From our previous papers,[1,3] we recall that the lowest excited state in TFB:F8BT and PFB:F8BT heterojunctions is a strongly bound charge-transfer (CT) state (exciplex state). However, since fluorescence emanates from the lowest excitonic (XT) state, we focus on these two states and investigate the interconversion rates between them.

Prior to discussing the kinetics, we briefly comment on the effect of chain length and interchain dielectric screening. We have noted that the interchain separation essentially modulates the interchain two-body interactions in recognition of the higher dielectric screening between chains compared to that between repeat units on the same chain. Thus, the interchain separation is a parametric equivalent of the interchain screening length ,which largely affects the CI eigenenergies calculated particularly for the lowest CT and XT states and thus modulates the calculated binding energy. It is for this particular reason that we tune this screening length such that the calculated CT-XT energy difference corresponds to that observed in experiments. Shown in Figure 5 is the variation with respect to interchain screening length (given in terms of r_0) of the energies of the lowest vertical as well as relaxed CI states of TFB:F8BT with 3 and 9 copolymers on each chain, respectively. Here we observe a couple of things. First, the CT states have greater sensitivity to the interchain screening length compared to the XT states. This is expected since CT configurations involve not only intrachain electron−hole pairs but also interchain electron−hole pairs as opposed to XT configurations which are purely intrachain electron−hole pairs. The calculated vertical and relaxed energies of isolated F8BT having 9 copolymer units is

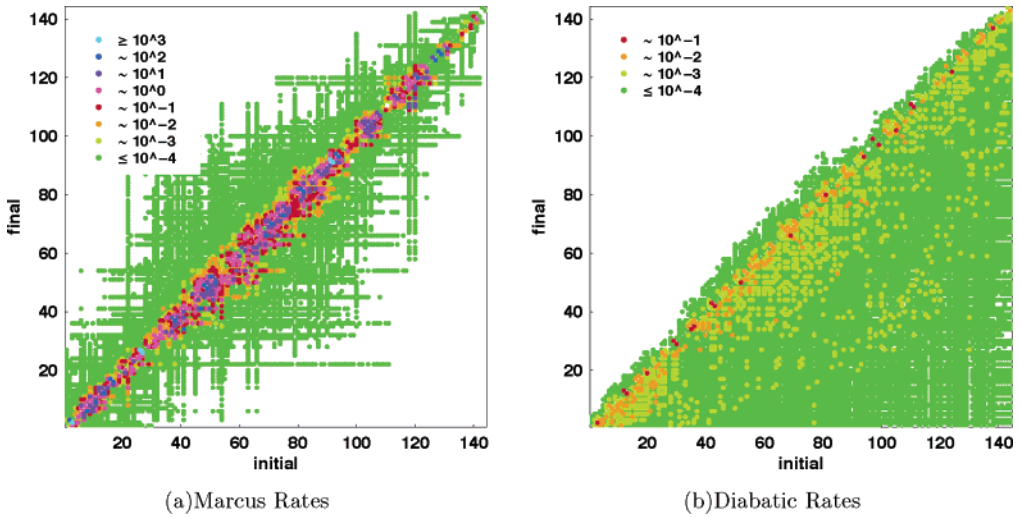

Figure 7. TFB-F8BT internal conversion rate distribution at 290 K. Rates are in ps^{-1}. Note the sparsity and relatively faster Marcus rates compared to the diabatic rates.

2.29 and 2.13 eV, respectively. While the vertical XT state of TFB:F8BT is at 2.29 eV, the relaxed XT state is slightly higher than that of the isolated F8BT. This is due to significant mixing between this state and the lowest vertical CT state, particularly, at screening lengths less than 2. Consequently, the relaxed XT state of TFB:F8BT has significant charge-transfer character as seen in Figure 6. For PFB:F8BT (not shown), the vertical and relaxed XT states are at the same values as that of the isolated F8BT for screening lengths up to 2. Moreover, increasing the number of repeat units of the F8BT chain leads to a slight decrease in the vertical CT and XT energies. The XT, however, is more sensitive to this increase in chain length as the excitons are localized in the F8BT leading to a decrease in the CT-XT energy difference. Increasing the length of the TFB chain, on the other hand, leads to a sizable decrease in the vertical CT energy while having practically no effect on the XT energy leading to an increase in the CT-XT energy difference. Again, this is expected as the CT states consist of electrons and holes localized at F8BT and TFB, respectively. In what follows, we consider interchain separations (screening lengths) of 1.4 and 1.2 for TFB:F8BT and PFB:F8BT, respectively. This gives vertical and relaxed CT-XT energy differences of 80 and 116 meV for the former and 346 and 306 meV for the latter, respectively. These are reasonably consistent with measurements by Morteani et al.[7,8] While we use a model with 3 copolymer units of TFB/PFB cofacially stacked with 9 copolymer units of F8BT to have maximum π-stacking between the two chains, slight changes in the chain lengths coupled with the appropriate adjustment of the interchain separation to generate the observed CT-XT energy difference would give consistent results to what we subsequently present.

A. Interconversion Dynamics. In calculating the state-to-state interconversion rates for TFB:F8BT, we note two major differences between the diabatic and the Marcus−Hush approaches (see Figure 7). First is the sparsity of the latter with transitions being limited to states with smaller energy differences. This leads to a relaxation dynamics that is more intertwined with the density of states (DOS). Second is the relatively faster rates calculated in the latter leading to interconversion lifetimes in the femtosecond (fs) to a couple of picosecond (ps) regime as opposed to hundreds of picoseconds in the former. The same general difference is observed for PFB:F8BT (not shown). These marked differences in the distribution of rates and their range of magnitudes are brought about by the introduction of the reorganization energy as a parameter in the rates calculation to complement the energy differences between the states. It provides a way to incorporate lattice distortions in the semiclassical limit into the relaxation dynamics. While this is not fully dynamical in its account of the lattice distortions, it improves upon the diabatic approximation previously employed.

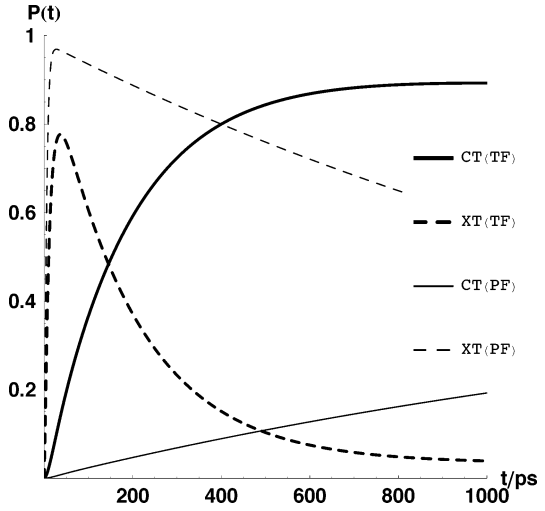

Figure 8. Time-evolved populations of the lowest CT (solid lines) and XT (dashed lines) vertical states of TFB:F8BT (TF) and PFB:F8BT (PF) in the diabatic approximation at 290 K.

The photoexcitation of heterojunction systems is simulated by populating a higher lying excitonic state with a quanta of photon. Figures 8 and 9 show the time-evolved populations of the lowest charge-transfer (CT) and excitonic (XT) vertical and relaxed states, respectively, in photoexcited TFB:F8BT and PFB:F8BT. We see, in both approaches, that the relaxation to the lowest CT state is faster in TFB:F8BT than in PFB:F8BT. Furthermore, the relaxation from the XT state to the CT state occurs faster in the former. This is despite the XT state being formed faster in the latter for both cases. This is manifested more in the Marcus−Hush approach shown in Figure 9 where despite reaching a maximum population of 0.92 in 150 fs as opposed to just 0.72 in 950 fs (see inset), the XT → CT interconversion is practically done in 60 ps in TFB:F8BT compared to 600 ps in PFB:F8BT. In addition, we note that the XT state reaches a steady state population in TFB:F8BT whereas it practically goes to zero in PFB:F8BT. This small but nonzero

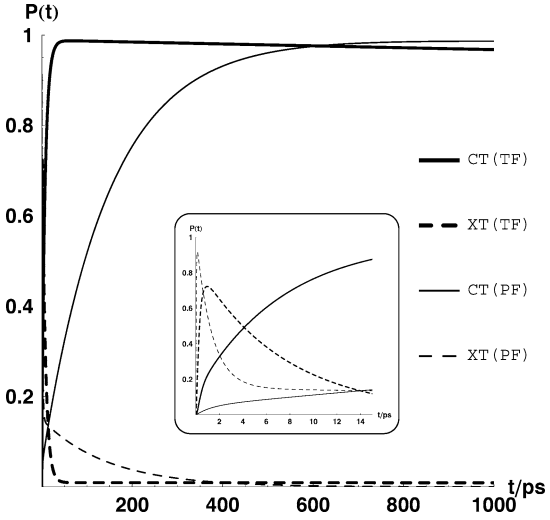

Figure 9. Time-evolved populations of the lowest CT (solid lines) and XT (dashed lines) relaxed states of TFB:F8BT (TF) and PFB:F8BT (PF) in the Marcus−Hush approach at 290 K. The inset shows the evolution at earlier times.

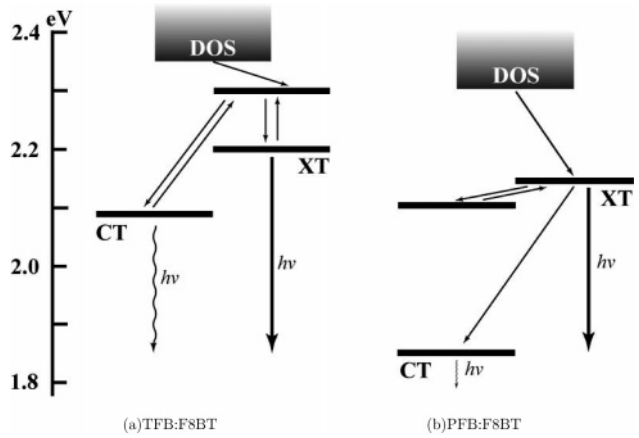

Figure 10. Relevant Marcus−Hush interconversion rates for the three lowest states of (a) TFB:F8BT and (b) PFB:F8BT. In both cases, relaxation proceeds from the density of states (DOS) to the lowest excitonic state (XT) (offset to the right relative to the CT states for clarity of relaxation route) before relaxing to the lowest charge-transfer state (CT). In PFB:F8BT, the intermediate state lies lower in energy relative to the lowest XT state and has a charge-transfer character. In TFB:F8BT, it has a higher energy with a more excitonic character. Also shown are the radiative rates emanating from the XT states which are strongly coupled to the ground state, S_0, of both systems and the CT states which are just weakly coupled to S_0.

population of the XT state is consistent with the distributed thermal population of states of 0.007 at 290 K because this XT state is 116 meV higher in energy relative to the lowest CT state.[1]

Interestingly, while the overall XT → CT interconversion occurs in just a couple of picoseconds in both heterojunction systems, a closer look into the rates reveals that this relaxation does not occur straightforwardly. Figure 10 shows the relevant interconversions between the three lowest states of both systems: the lowest CT state, the lowest XT state, and an intermediate state that is either higher or lower in energy relative to the XT state. In TFB:F8BT, it is higher and is excitonic while in PFB:F8BT it is lower and has a charge-transfer character. Figure 6 shows the electron/hole densities of these three lowest states for TFB:F8BT and PFB:F8BT. It is worth noting that there is considerable mixing between the intrachain and interchain configurations of the former compared to those of the

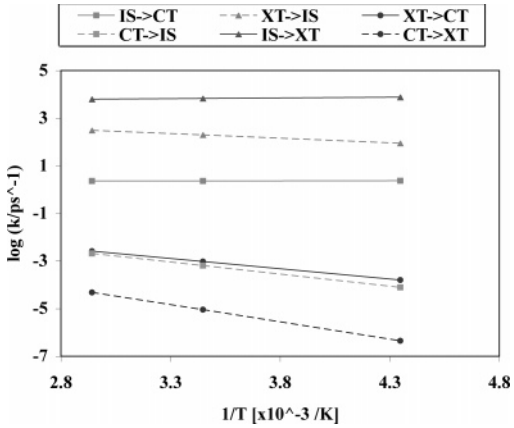

Figure 11. Interconversion rates between the three lowest states of TFB:F8BT calculated in the Marcus−Hush approximation as a function of temperature (230, 290, and 340 K). The plot is given as log(k/ps^{-1}) vs 1/T. Transitions to lower energy states are given as solid lines while their reverse are given as dashed lines. The IS ↔ CT, CT ↔ XT, and XT ↔ CT are plotted as squares, triangles, and circles, respectively. All transition rates increase directly with temperature except the IS → XT and IS → CT conversions which decrease as temperature increases.

latter. In TFB:F8BT (Figure 10), the direct XT → CT transition ($\sim 10^{-4}$ ps^{-1}) is at least 3 orders of magnitude slower than the corresponding indirect transition route (>1 ps^{-1}), the latter being consistent with the evolution data (Figure 9). Thus, the XT → CT conversion occurs via the intermediate state and not directly. The reverse transitions for both routes are slower but have relatively the same order of magnitude difference. This CT → XT transition via the intermediate state ($\sim 10^{-4}$ ps^{-1}) effectively presents a regeneration pathway for the XT. This leads to an XT state population that is always at equilibrium with the CT state.

In PFB:F8BT (Figure 10), the direct XT → CT interconversion is $\sim 10^{-2}$ ps^{-1} while the CT → XT rate is $\sim 10^{-7}$ ps^{-1}. The interconversion between CT and the intermediate state, on the other hand, is at least 5 orders of magnitude slower. Consequently, XT is not regenerated.

B. Effect of Temperature. To see the effect of temperature, the interconversion rates were calculated at 230, 290, and 340 K. Figure 11 shows how the interconversions among the three lowest states (CT, XT, and the intermediate state (IS)) of TFB:F8BT, as illustrated in Figure 10a, vary with temperature. This dependence is given in an Arrhenius plot of log k vs 1/T and gives a linear plot for each transition having a slope associated with the activation energy, E_{act}, for that particular transition. This activation energy has the expression,

$$E_{act} = \frac{(\Delta E - E_\lambda)^2}{4E_\lambda} \tag{20}$$

from eq 17. Transitions to lower energy states are given as solid lines while those going to higher energy states are given as dashed lines. Curiously, although XT → CT is exothermic compared to XT → IS, which is endothermic, the latter is a more favorable transition. This has to do with the fact that XT → CT has twice the activation energy as that of XT → IS.

Overall, in TFB:F8BT, we see an increase in the fraction of the total excited state population in XT as temperature increases. At 230 K only 0.3% is in XT while at 290 and 340 K, 1% and 2% is in XT, respectively.

The effect of temperature on the interconversion rates among the three lowest states of PFB:F8BT is given in Figure 12 in the same way as that of TFB:F8BT. Note that the CT → XT

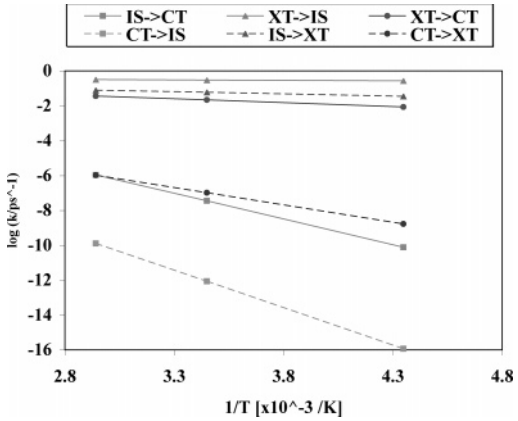

Figure 12. Interconversion rates between the three lowest states of PFB:F8BT calculated in the Marcus−Hush approximation as a function of temperature (230, 290, and 340 K). The plot is given as $\log(k/\mathrm{ps}^{-1})$ vs $1/T$. Transitions to lower energy states are given as solid lines while their reverse are given as dashed lines. The IS ↔ CT, IS ↔ XT, and XT ↔ CT are plotted as squares, triangles, and circles, respectively. All transition rates increase directly with temperature.

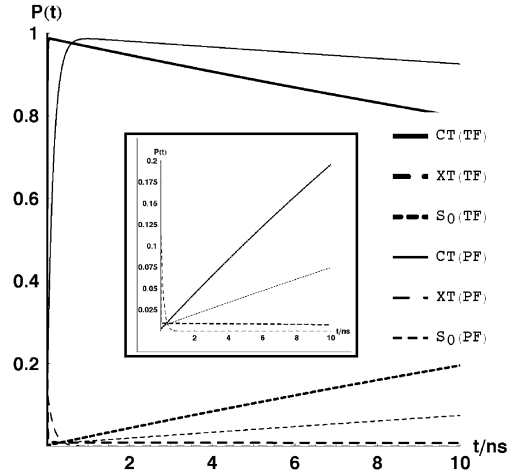

Figure 13. Time-evolved populations of the lowest CT, lowest XT, and ground state (S_0) of TFB:F8BT (bold plots) and PFB:F8BT from initially populated lowest XT at 290 K. The radiative rate of XT is 2 orders of magnitude greater than that of CT.

(dashed circles) and CT → IS (dashed squares) are marginal even at 340 K. This lack of competitive transitions from the CT to the higher lying states led to poor luminescence properties.

Finally, we note that all transition rates increase with temperature except for the IS → XT and IS → CT in TFB:F8BT which decrease with temperature. Such a trend, while not uncommon in chemical reactions, is though to be indicative of a more complicated transition mechanism as noted by Porter.[23] We surmise this to be due to the coupling between the low-frequency vibrational modes of the initial state with the high-frequency vibrational modes of the final state as in the case of an early transition state in reactive scattering.

C. Radiative Decay. The photoluminescence of TFB:F8BT and PFB:F8BT is simulated by incorporating the radiative rates and evolving the populations at long time scale (in the nanosecond (ns) regime). Figure 13 shows the time-evolved populations of the lowest CT and XT states as well as the ground state (S_0) to 10 ns at 290 K. We note that the radiative decay from XT for TFB:F8BT (0.131 ns^{-1}) and PFB:F8BT (0.139 ns^{-1}) is about 2 orders of magnitude greater than that from CT. However, due to the aforementioned existence of a steady state between CT and XT in TFB:F8BT as illustrated in Figure 10a, the XT is regenerated to maintain 1% of the excited-state population. Consequently, 11% of the decay population to S_0 comes from XT when integrated over time. At 230 K, only 4% of the decay population comes from XT while at 340 K, 20% comes from XT. This increasing fraction of the total decay population emanating from XT coupled with the increasing fraction of the total excited-state population residing in XT leads to an overall increase in the population of S_0 as temperature increases. This increase in the photoluminescence from the F8BT in the TFB:F8BT blend with temperature is consistent with what has been observed in the temperature-dependent, time-resolved spectroscopic studies done by Morteani et al.[7,8] on this material. For PFB:F8BT, on the otherhand, 99.98% of the decay population emanates from the CT state. Even at 340 K, only 1% of the decay emanates from the XT state. Consequently, PFB:F8BT exhibit poor photoluminescent properties.

IV. Conclusion

Using the Marcus−Hush approach, we have successfully introduced lattice reorganization into our exciton model and simulated excited state relaxations that are consistent with experiments. In this paper, we have demonstrated that suitably constructed type II heterojunction systems may lead to materials that exhibit good photovoltaic behavior due to the formation of charge-separated states across the heterojunction while at the same time also show luminescent properties via the presence of an exciton regeneration pathway. We have demonstrated that in cofacially stacked heterojunctions this pathway is not a direct conversion from the lowest CT state to the lowest XT state but rather involves intermediate states. While we see indications that this pathway is model sensitive, we consistently determine the CT state to be the lowest excited state and that the regeneration of the lowest XT state depends largely on its thermal accessibility from the CT state.

Finally, we have not explicitly considered the effect of surrounding dielectric media. Solvents have been shown to have a profound impact upon polymer morphology and aggregation, particularly at the interface between two polymer phases.[34,35] In this regard, its exact role, as well as the exact geometries at the interface, remains an open question. Furthermore, solvents have exhibited screening effects that serve to modify the interaction between adjacent polymer phases. Since we have dealt with materials that have low dielectric constants and since common solvents used in the preparation of these polymer blends also have low dielectric constants, we expect solvent polarizability to have a minimal effect. However, consideration of these and other external effects is not without merit and should eventually be considered.

Acknowledgment. This work was supported in part by the National Science Foundation and the Robert A. Welch Foundation. J.G.S.R. thanks Dr. Stoyan Karabunarliev for his guidance and invaluable contributions to this project.

References and Notes

(1) Bittner, E. R.; Ramon, J. G. S.; Karabunarliev, S. *J. Chem. Phys.* **2005**, *122*, 214719; URL http://link.aip.org/link/?JCP/122/214719/1.

(2) Karabunarliev, S.; Bittner, E. R. *J. Chem. Phys.* **2003**, *118*, 4291; URL http://link.aip.org/link/?JCP/118/4291/1.

(3) Karabunarliev, S.; Bittner, E. R. *J. Phys. Chem. B* **2004**, *108*, 10219; URL http://dx.doi.org/10.1021/jp036587w.

(4) Karabunarliev, S.; Bittner, E. R. *Phys. Rev. Lett.* **2003**, *90*, 057402; URL http://link.aps.org/abstract/PRL/v90/e057402.

(5) Jenekhe, S. A.; Yi, S. *Appl. Phys. Lett.* **2000**, *77*, 2635; URL http://link.aip. org/link/?APL/77/2635/1.

(6) Alam, M. M.; Jenekhe, S. A. *Chem. Mater.* **2004**, *16*, 4647; URL http://dx.doi. org/10.1021/cm0497069.

(7) Morteani, A. C.; Dhoot, A. S.; Kim, J.-S.; Silva, C.; Greenham, N. C.; Murphy, C.; Moons, E.; Ciná, S.; Burroughes, J. H.; Friend, R. H. *Adv. Mater.* **2003**, *15*, 1708; URL http: //dx.doi.org/10.1002/adma.200305618.

(8) Morteani, A. C.; Sreearunothai, P.; Herz, L. M.; Friend, R. H.; Silva, C. *Phys. Rev. Lett.* **2004**, *92*, 247402; URL http://link.aps.org/abstract/PRL/v92/e247402.

(9) Heun, S.; Mahrt, R. F.; Greiner, A.; Lemmer, U.; Bassler, H.; Halliday, D. A.; Bradley, D. D. C.; Burn, P. L.; Holmes, A. B. *J. Phys.*: *Condens. Matter* **1993**, *5*, 247; URL http://www.iop.org.ezproxy.lib.uh.edu/EJ/abstract/0953-8984/5/2/012.

(10) BrÈdas, J.-L.; Cornil, J.; Heeger, A. J. *Adv. Mater.* **1996**, *8*, 447; URL http: //dx.doi.org/10.1002/adma.19960080517.

(11) Cao, Y.; Parker, I. D.; Yu, G.; Zhang, C.; Heeger, A. J. *Nature* **1999**, *397*, 414; URL http://dx.doi.org/10.1038/17087.

(12) Cornil, J.; Gueli, I.; Dkhissi, A.; Sancho-Garcia, J. C.; Hennebicq, E.; Calbert, J. P.; Lemaur, V.; Beljonne, D.; Bredas, J. L. *J. Chem. Phys.* **2003**, *118*, 6615; URL http: //link.aip.org/link/?JCP/118/6615/1.

(13) Jespersen, K. G.; Beenken, W. J. D.; Zaushitsyn, Y.; Yartsev, A.; Andersson, M.; Pullerits, T.; Sundstrom, V. *J. Chem. Phys.* **2004**, *121*, 12613; URL http://link.aip. org/link/?JCP/121/12613/1.

(14) Stevens, M. A.; Silva, C.; Russell, D. M.; Friend, R. H. *Phys. Rev. B*: *Condens. Matter Mater. Phys.* **2001**, *63*, 165213; URL http://link.aps.org/abstract/PRB/v63/e165213.

(15) Vogl, P.; Campbell, D. K. *Phys. Rev. B* **1990**, *41*, 12797; ISSN 18, URL http: //link.aps.org/abstract/PRB/v41/p12797.

(16) Yu, Z. G.; Wu, M. W.; Rao, X. S.; Sun, X.; Bishop, A. R. *J. Phys.*: *Condens. Matter* **1996**, *8*, 8847; ISSN 45, URL http://www.iop.org.ezproxy.lib.uh.edu/EJ/abstract/0953-8984/8/45/018.

(17) Khan, A. L. T.; Sreearunothai, P.; Herz, L. M.; Banach, M. J.; Kohler, A. *Phys. Rev. B*: *Condens. Matter Mater. Phys.* **2004**, *69*, 085201; URL http://link. aps.org/abstract/PRB/v69/e085201.

(18) Wells, J.-P. R.; Lidzey, D. G.; Phillips, P. J.; Carder, D. A.; Fox, A. M. *Appl. Phys. Lett.* **2004**, *85*, 3080; URL http://link.aip.org/link/?APL/85/3080/1.

(19) Guha, S.; Rice, J. D.; Yau, Y. T.; Martin, C. M.; Chandrasekhar, M.; Chandrasekhar, H. R.; Guentner, R.; de Freitas, P. S.; Scherf, U. *Phys. Rev. B*: *Condens. Matter Mater. Phys.* **2003**, *67*, 125204; URL http://link.aps.org/abstract/PRB/v67/e125204.

(20) Tretiak, S.; Saxena, A.; Martin, R. L.; Bishop, A. R. *Phys. Rev. Lett.* **2002**, *89*, 097402; URL http://link.aps.org/abstract/PRL/v89/e097402.

(21) Karabunarliev, S.; Bittner, E. R. *J. Chem. Phys.* **2003**, *119*, 3988; URL http://link.aip.org/link/?JCP/119/3988/1.

(22) Karabunarliev, S.; Bittner, E. R. *Phys. Rev. Lett.* **2003**, *90*, 079901; URL http://link.aps.org/abstract/PRL/v90/e079901.

(23) Lanzani, G.; Cerullo, G.; Polli, D.; Gambetta, A.; Zavelani-Rossi, M.; Gadermaier, C. *Phys. Status Solidi A* **2004**, *201*, 1116; URL http://dx.doi.org/10.1002/pssa.200404337.

(24) Gadermaier, C.; Lanzani, G. *J. Phys.*: *Condens. Matter* **2002**, *14*, 9785; URL http://stacks.iop.org/0953-8984/14/9785.

(25) Lanzani, G.; Cerullo, G.; Brabec, C.; Sariciftci, N. S. *Phys. Rev. Lett.* **2003**, *90*, 047402; URL http://link.aps.org/abstract/PRL/v90/e047402.

(26) Kersting, R.; Lemmer, U.; Mahrt, R. F.; Leo, K.; Kurz, H.; Bässler, H.; Göbel, E. O. *Phys. Rev. Lett.* **1993**, *70*, 3820; URL http://link.aps.org/abstract/PRL/v70/p3820.

(27) Marcus, R. A. *Rev. Mod. Phys.* **1993**, *65*, 599; URL http://link.aps.org/abstract/RMP/v65/p599.

(28) Hush, N. S. *Electrochim. Acta* **1968**, *13*, 1005.

(29) May, V.; Kühn, O. *Charge and Energy Transfer Dynamics in Molecular Systems*, 2nd ed.; Wiley-VCH: New York, 2004.

(30) Barford, W.; Bursill, R. J.; Smith, R. W. *Phys. Rev. B*: *Condens. Matter Mater. Phys.* **2002**, *66*, 115205; URL http://link.aps.org/abstract/PRB/v66/e115205.

(31) Allinger, N. L.; Li, F.; Yan, L.; Tai, J. C. *J. Comput. Chem.* **1990**, *11*, 868; URL http://dx.doi.org/10.1002/jcc.540110709.

(32) Hehre, W. J. *A guide to molecular mechanics and quantum chemical calculations*; Wavefunction, 2003.

(33) Porter, G. *Nobel Lecture* **1967**, 241−263.

(34) Hu, D.; Yu, J.; Wong, K.; Bagchi, B.; Rossky, P. J.; Barbara, P. F. *Nature* **2000**, *405*, 1030; URL http://www.nature.com/nature/journal/v405/n6790/abs/4051030a0 fs.html.

(35) Nguyen, T.-Q.; Doan, V.; Schwartz, B. J. *J. Chem. Phys.* **1999**, *110*, 4068; URL http://link.aip.org/link/?JCP/110/4068/1.